Journal of Engineering Physics and Thermophysics, Vol. 76, No. 1, 2003

INVESTIGATION OF THE PERFORMANCE OF A SPIRAL-COIL FINNED TUBE HEAT EXCHANGER UNDER DEHUMIDIFYING CONDITIONS

P. Naphon and S. Wongwises

UDC 621.184.64

In the present study, heat-transfer characteristics of spiral-coil finned tube heat exchangers under dehumidifying conditions are investigated. A mathematical model of Ho et al. is modified by including fin efficiency. The derivation and solution methodologies are explained in detail. The effects of various inlet conditions of fluids flowing through the heat exchanger are discussed. The agreement of the model with the experimental data is satisfactory, with an average error of 1.2 and 4.0% for enthalpy and humidity effectivenesses, respectively.

1. Introduction. Heat exchangers are devices used to implement the heat exchange of two fluids that are at different temperatures. They have been used in a wide variety of applications: heat recovery processes, air conditioning and refrigeration systems, chemical reactors, and food and dairy processes. The design and analysis of curved-tube heat exchangers have been studied both analytically and experimentally, mostly for helical-coil heat exchangers [1–7].

The spiral-coil heat exchanger has received comparatively little attention in the literature. Some of the earliest works were performed by Ho et al. [8], who performed experimental and theoretical investigations on a compact spiral-coil heat exchanger. Unmixed and mixed air flow models were considered. The experiments were performed in a water flow rate range from 0.06 to 0.13 kg/sec and an air flow rate of 0.45 kg/sec. The inlet air temperature was from 50 to 70^{o}C. Ho and Wijeysundera [9, 10] presented experimental investigations on the thermal performance of the spiral-coil heat exchanger under cooling and dehumidifying conditions. The experimental studies were conducted at various air and water flow rates.

Relatively little information in the open literature, however, is currently available on heat-transfer characteristics in spiral-coil heat exchangers. In the present study, the main concern is to analyze the performance and to study the heat-transfer characteristics of spiral-coil finned and tube heat exchangers under dehumidifying conditions. The effects of relevant parameters are also investigated.

2. Mathematical Modeling. The mathematical model includes the effects of the in-tube heat-transfer coefficient, fin efficiency, and initial inlet conditions of both fluids flowing through the heat exchanger. The basic physical equations used to describe the flow characteristics are developed from the conservation equations of mass and energy. The model is based on that of Ho et al. [8–10] with the following assumptions:

– flows of air and water are steady;
– air humidity ratio at the outlet of each coil turn is equal;
– air-side convective heat-transfer coefficient at the outlet of each coil turn is equal;
– thermal resistance of the liquid film is neglected;
– each coil turn is approximately circular.

The flow of fluids in a spiral-coil heat exchanger takes place on two sides, the hot (gas) side and the cold (liquid) side. Air and water are used as working fluids. Figure 1 shows a schematic diagram of a typical spiral-coil cooling heat exchanger.

2.1. Air-side Heat Transfer. When air of one condition passes over a cooling coil having a coil surface temperature below the dew-point temperature of the air, the air is chilled below its dew-point, thus condensing out moisture. Considering the control volume of each segment as shown in Fig. 2, we represent the total heat-transfer rate as the sum of latent and sensible heat as follows:

Fluid Mechanics, Thermal Engineering and Multiphase Flow Research Laboratory (FUTURE), Department of Mechanical Engineering, King Mongkut's University of Technology, Thonburi, Bangmod, Bangkok 10140, Thailand. Tel.: +662-470-9115; Fax: +662-470-9111; email: somchai.won@kmutt.ac.th. Published in Inzhenerno-Fizicheskii Zhurnal, Vol. 76, No. 1, pp. 71–79, January–February, 2003.

1062-0125/03/7601-0083$25.00

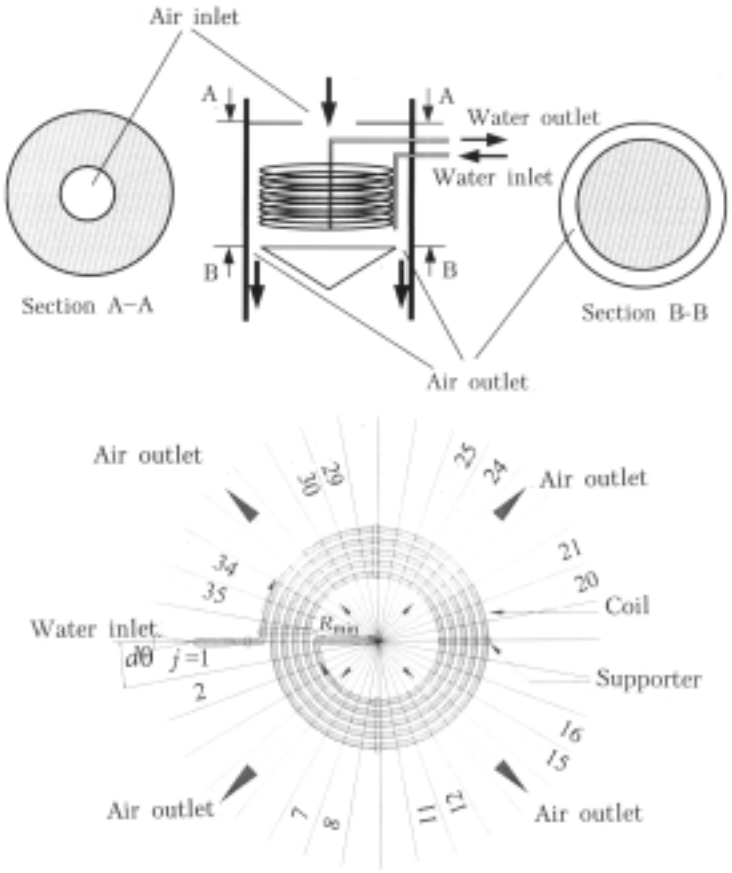

Fig. 1. Schematic diagram of a spiral-coil exchanger.

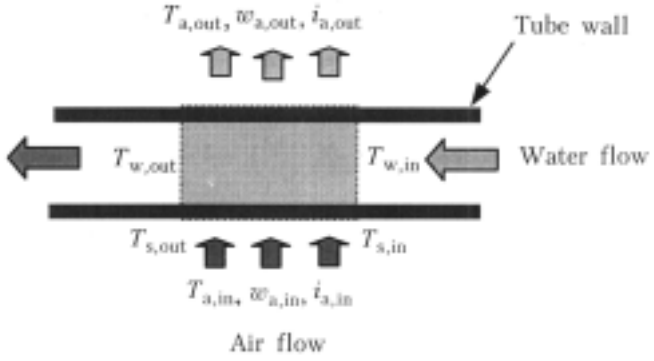

Fig. 2. Control volume of each segment.

$$dQ_T = dQ_S + dQ_L \,, \tag{1}$$

where dQ_T, dQ_S, and dQ_L are the total heat, sensible heat, and latent heat, respectively,

$$dQ_S = h_a \,(dA_b + \eta dA_f)\,(T_{a,in} - T_s) \,, \tag{2}$$

where h_a is the air-side heat-transfer coefficient, dA_b is the outside surface area excluding the area of the fins, dA_f is the surface area of the fins, η is the fin efficiency, $T_{a,in}$ is the inlet air temperature, and T_s is the tube surface temperature.

As the moisture is condensed, the heat released is given by the following latent heat-transfer rate:

$$dQ_L = dm_{wv} i_{con} \,, \tag{3}$$

where i_{con} is the enthalpy of condensation and dm_{wv} is the mass transfer rate of the water vapor, defined as

$$dm_{wv} = h_{mass}\,(dA_b + \eta dA_f)\,(w_{a,in} - w_{sat,s})\,, \tag{4}$$

where h_{mass} is the mass-transfer coefficient, $w_{a,in}$ is the inlet humidity ratio of air, and $w_{sat,s}$ is the humidity ratio at saturated conditions at the tube surface temperature.

Substituting Eqs. (2), (3), and (4) into Eq. (1) gives

$$dQ_T = h_a\,(dA_b + \eta dA_f)\,(T_{a,in} - T_s) + h_{mass}(dA_b + \eta dA_f)\,(w_{a,in} - w_{sat,s})\,i_{con}\,. \tag{5}$$

Equation (5) can be arranged in the following form:

$$dQ_T = \frac{h_a}{C_{pm}}\,(dA_b + \eta dA_f)\left[C_{pm}\,(T_{a,in} - T_s) + \frac{1}{Le}\,(w_{a,in} - w_{sat,s})\,i_{con}\right], \tag{6}$$

where the Lewis number Le is defined by $Le = \dfrac{h_a}{h_{mass}C_{pm}}$.

The specific heat of the moist air C_{pm} is the sum of the specific heat of dry air and water vapor:

$$C_{pm} = C_p + w_a C_{pwv}\,. \tag{7}$$

Substituting Eq. (7) into Eq. (6) and assuming Le approximately equal to 1, we get

$$dQ_T = \frac{h_a\,(dA_b + \eta dA_f)}{C_{pm}}\,(i_{a,in} - i_{sat,s})\,, \tag{8}$$

where $i_{a,in}$ is the inlet enthalpy of air and $i_{sat,s}$ is the enthalpy at saturated conditions at the tube surface temperature.

2.2. Water-side Heat Transfer. The heat-transfer rate in terms of the water flow rate can be given as

$$dQ_T = m_w C_{pm} dT_w\,. \tag{9}$$

The heat-transfer rate to the water can be expressed as

$$dQ_T = h_{com}\,(dA_b + \eta dA_f)\,(T_s - T_w)\,, \tag{10}$$

where

$$\frac{1}{h_{com}} = \frac{x\,(dA_b + \eta dA_f)}{kA_{ave}} + \frac{dA_b + \eta dA_f}{h_i A_i}\,, \tag{11}$$

where x is the tube thickness, A_{ave} is the average surface area, and h_{com} is the combined conductance through the tube surface and water inside tube.

2.3. Energy Balance. Considering the energy balance over the control volume for each segment, we get

$$\frac{h_a\,(dA_b + \eta dA_f)}{C_{pm}}\,(i_{a,in} - i_{sat,s}) = h_{com}\,(dA_b + \eta dA_f)\,(T_s - T_w)\,. \tag{12}$$

Rearranging gives

$$\frac{h_a}{h_{com}C_{pm}} = \frac{T_s - T_w}{i_{a,in} - i_{sat,s}} = Rc\,. \tag{13}$$

The enthalpy of the saturated air $i_{sat,s}$ at the wet surface temperature in Eq. (13) as proposed by Goodman [10] is as follows:

$$i_{sat,s} = 10.90748 + 1.22045T_s + 0.05652T_s^2 . \tag{14}$$

Substituting Eq. (14) into Eq. (13) and rearranging, we get

$$0.05652T_s^2 + \left(1.22045 + \frac{1}{Rc}\right)T_s + \left(10.90749 - i_{a,in} - \frac{T_w}{Rc}\right) = 0 . \tag{15}$$

The energy balance over the control volume for each segment may be written in terms of the water flow rate as follows:

$$h_{com}\,(dA_b + \eta dA_f)\left(\frac{T_{s,out} + T_{s,in}}{2} - \frac{T_{w,out} + T_{w,in}}{2}\right) = m_w C_{pw}\,(T_{w,out} - T_{w,in}) . \tag{16}$$

On rearranging, we get

$$T_{w,out} = \frac{1}{\beta + 1}\left[\beta\,(T_{s,out} + T_{s,in}) - T_{w,in}\,(\beta - 1)\right], \tag{17}$$

where

$$\beta = \frac{h_{com}\,(dA_b + \eta dA_f)}{2m_w C_{pw}} . \tag{18}$$

Equation (15) can be written using $T_{s,out}$ and $T_{s,in}$, so

$$0.05652T_{s,out}^2 + \left(1.22045 + \frac{1}{Rc}\right)T_{s,out} + \left(10.90749 - i_{a,in} - \frac{T_{w,out}}{Rc}\right) = 0 \tag{19}$$

and

$$0.05652T_{s,in}^2 + \left(1.22045 + \frac{1}{Rc}\right)T_{s,in} + \left(10.90749 - i_{a,in} - \frac{T_{w,in}}{Rc}\right) = 0 . \tag{20}$$

Substituting Eq. (17) into Eq. (19) then gives

$$0.05652T_{s,out}^2 + \left[1.22045 + \frac{1}{Rc} - \frac{\beta}{Rc\,(\beta + 1)}\right]T_{s,out}$$

$$+ 10.90749 - i_{a,in} - \frac{1}{Rc\,(\beta + 1)}\left[\beta T_{s,in} - (\beta - 1)\,T_{w,in}\right] = 0 . \tag{21}$$

2.4. Fin Efficiency. The fin efficiency is defined as the ratio of the actual heat transfer to the ideal heat transfer through the fin when the entire fin is at base temperature. For a fin with uniform cross section and insulated at the fin tip, the fin efficiency can be determined from

$$\eta = \frac{\tanh\,(Mr_o\phi)}{Mr_o\phi}, \tag{22}$$

where

$$M = \left(\frac{2h_a}{ky}\right)^{1/2}, \quad \phi = \left(\frac{R_f}{r_o} - 1\right)\left[1 + 0.35\ln\left(\frac{R_f}{r_o}\right)\right], \tag{23}$$

where k is the thermal conductivity of the fins, y is the fin thickness, r_o is the outer radius of the tube, and R_f is the radius of the annular fins.

Equation (23) is appropriate for a dry fin surface. However, for a wet fin surface, the equation developed by McQuiston [11] can be used to determine the fin efficiency:

$$M^2 = \frac{2h_{\mathrm{a}}}{ky}\left(1 + \frac{C_{\mathrm{sa}} i_{\mathrm{con}}}{C_{p\mathrm{m}}}\right), \tag{24}$$

$$C_{\mathrm{sa}} = \frac{1}{2}\left(\frac{w_{\mathrm{sat,w,out}} - w_{\mathrm{a,in}}}{T_{\mathrm{w,out}} - T_{\mathrm{a,in}}} + \frac{w_{\mathrm{sat,w,in}} - w_{\mathrm{a,out}}}{T_{\mathrm{w,in}} - T_{\mathrm{a,out}}}\right) \cong \frac{w_{\mathrm{sat,s}} - w_{\mathrm{a}}}{T_{\mathrm{s}} - T_{\mathrm{a}}}\,. \tag{25}$$

The specific humidity $w_{\mathrm{sat,s}}$ of air at saturated conditions is a function of inlet and outlet surface temperatures and can be obtained from the correlation given by Liang [12, 13]:

$$w_{\mathrm{sat,s}} = (3.7444 + 0.3078T_{\mathrm{s}} + 0.0046T_{\mathrm{s}}^2 + 0.0004T_{\mathrm{s}}^3) \times 10^{-3}\,, \quad 0 < T_{\mathrm{s}} < 30^{\mathrm{o}}\mathrm{C}\,. \tag{26}$$

2.5. Thermal Performance of Spiral-Coil Heat Exchanger. The enthalpy effectiveness and humidity effectiveness are used to evaluate the total cooling load and latent load removal performance of the coil, respectively, as follows:

enthalpy effectiveness

$$E_i = \frac{i_{\mathrm{a,in}} - i_{\mathrm{a,out}}}{i_{\mathrm{a,in}} - i_{\mathrm{sat,s,in}}}, \tag{27}$$

humidity effectiveness

$$E_w = \frac{w_{\mathrm{a,in}} - w_{\mathrm{a,out}}}{w_{\mathrm{a,i}} - w_{\mathrm{sat,s,in}}}\,. \tag{28}$$

2.6. Correlations for Heat-Transfer Coefficients. A correlation proposed by McQuiston [11] to predict the air-side heat-transfer coefficient for the wet fin-tube surface is as follows:

$$h_{\mathrm{a}} = \frac{JGC_{p\mathrm{m}}}{\mathrm{Pr}_{\mathrm{o}}^{2/3}}\,, \tag{29}$$

where

$$J = 0.38\,\mathrm{Re}_{\mathrm{o}}^{-0.4}\left(\frac{A_{\mathrm{b}} + \eta A_{\mathrm{f}}}{A_{\mathrm{b}}}\right)^{-0.15}\left(0.84 + 4\cdot 10^{-5}\,\mathrm{Re}_{\mathrm{fs}}^{1.25}\right). \tag{30}$$

The correlation proposed by Mori and Nakayama [10] to evaluate the in-tube heat-transfer coefficient is as follows:

for laminar flow,

$$\mathrm{Nu}_{\mathrm{i}} = \frac{0.864}{\zeta}\,\mathrm{De}^{0.5}\left(1 + 2.35\mathrm{De}^{-0.5}\right), \tag{31}$$

where

$$\mathrm{De} = \mathrm{Re}_{\mathrm{i}}\left(\frac{D_{\mathrm{i}}}{D_{\mathrm{c}}}\right)^{0.5}\,, \tag{32}$$

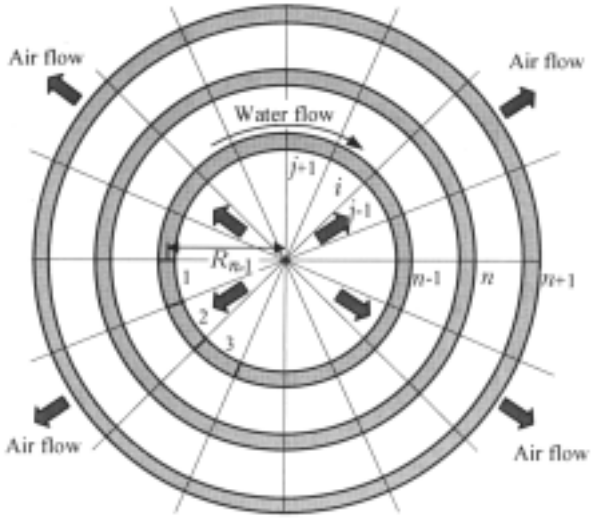

Fig. 3. Schematic diagram of simulation approach.

$$\zeta = \frac{2}{11}\left(1 + \sqrt{1 + \frac{77}{4}\frac{1}{\mathrm{Pr}_\mathrm{i}^2}}\right) \quad \text{for} \quad \mathrm{Pr}_\mathrm{i} > 1\,; \tag{33}$$

for turbulent flow,

$$\mathrm{Nu}_\mathrm{i} = \frac{\mathrm{Pr}_\mathrm{i}\,\mathrm{Re}_\mathrm{i}^{4/5}\left(\dfrac{D_\mathrm{i}}{D_\mathrm{c}}\right)^{0.1}}{26.2\,(\mathrm{Pr}_\mathrm{i}^{2/3} - 0.074)}\left(1 + \frac{0.098}{\left[\mathrm{Re}_\mathrm{i}\left(\dfrac{D_\mathrm{i}}{D_\mathrm{c}}\right)^2\right]^{1/5}}\right), \quad \mathrm{Re}_\mathrm{i}\left(\frac{D_\mathrm{i}}{D_\mathrm{c}}\right)^2 > 0.1\,. \tag{34}$$

The critical Reynolds number correlation as proposed by Srinivasan et al. [6] is

$$\mathrm{Re}_\mathrm{cr} = 2100\left[1 + 12\left(\frac{D_\mathrm{i}}{D_\mathrm{c}}\right)^{0.5}\right]. \tag{35}$$

3. Calculation Procedure. The spirally coiled tube is divided into numerous layers of circular coils with the following mean radius:

$$R_n = \frac{1}{2\pi}\int_0^{2\pi} R\,d\theta \tag{36}$$

or

$$R_n = [R_\mathrm{min} + (2n - 1)\,\alpha\pi]\,, \tag{37}$$

where R_min is the minimum coil radius, n is the number of coil turns, and α is the rate of radius change per radian.

Each layer of circular coil turn can be divided into numerous sections, as shown in Fig. 3. Since the thermodynamic properties of fluids at both inlet sections are known, the calculation is done section by section along the curved tube, which begins at the first section of the innermost coil turn. For each section, the inlet water temperature $T_\mathrm{w,in}$, outlet water temperature $T_\mathrm{w,out}$, inlet surface temperature $T_\mathrm{s,in}$, and outlet surface temperature $T_\mathrm{s,out}$ are deter-

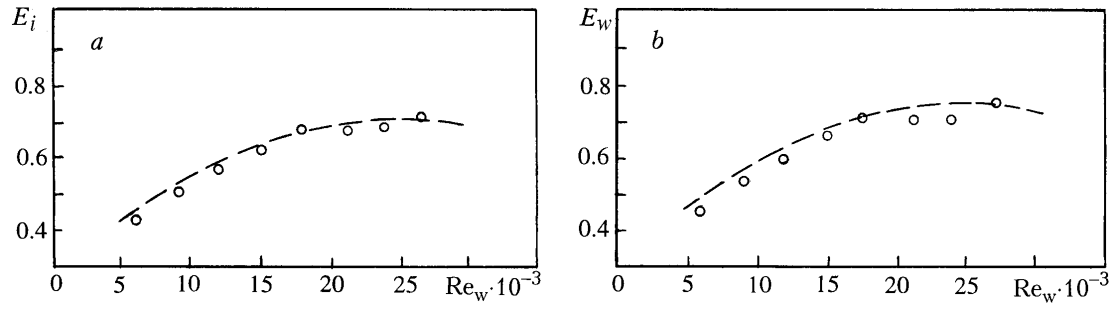

Fig. 4. Comparison of present numerical results (dashed curves) and experimental (Ho) data (points) for enthalpy (a) and humidity (b) effectivenesses at $T_{a,in}$ = 26.5°C, $T_{w,in}$ = 5.5°C, m_a = 0.231 kg/sec, w_{in} = 0.02, and n = 8.

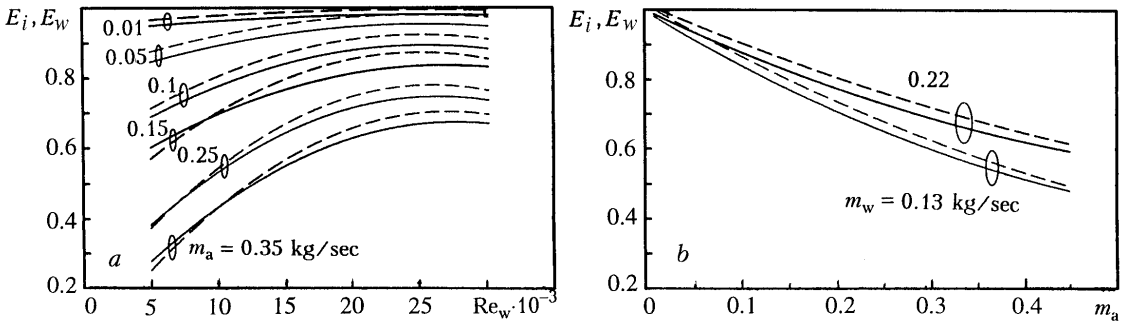

Fig. 5. Variation of enthalpy (solid curves) and humidity (dashed curves) effectivenesses with water Reynolds number (a) and air flow rate (b) at $T_{a,in}$ = 30°C, $T_{w,in}$ = 8°C, w_{in} = 0.02, and n = 10. m_a, kg/sec.

mined from Eqs. (17), (20), and (21) by using the Newton–Raphson iterative technique. The fin efficiency η, total heat Q_T, latent heat Q_L, sensible heat Q_S, air-side heat-transfer coefficient h_a, and in-tube heat-transfer coefficients h_i, are then computed.

4. Results and Discussion. Even though the present model is based on that of Ho et al. [10], there are a number of important differences, which are as follows:

– The present model uses Srinivasan's correlation [6] to determine the critical Reynolds number for flow in the curved tube, whereas the model of Ho et al. uses Ito's correlation [10].

– The present model uses the in-tube heat-transfer coefficient correlation of Mori and Nakayama [6], whereas the Ho et al. model uses Rogers and Mayhew's correlation [10].

– The variables of each control volume are determined by using the Newton–Raphson iterative technique.

– The fin efficiency is included in the calculation procedure.

– The forward computational procedure is used in this model, whereas the model of Ho et al. uses the backward computational procedure.

– The present model uses the specific humidity correlation of air at saturated conditions given by Liang [12, 13].

The present model allows for a number of parameters to be included for any given computation. Inlet water and air temperatures and water and air flow rates were each varied to investigate their effect on the performance and heat and mass transfer characteristics of spiral-coil cooling heat exchangers under dehumidifying conditions. In order to validate the present model, comparisons were made with limited available measured data.

Figures 4a and b compare the simulation results of enthalpy and humidity effectivenesses from the present model with the experimental data of Ho and Wijeysundera [10]. It can be noted that for a water Reynolds number <25,000 the effectivenesses of enthalpy and humidity increase rapidly with the water Reynolds number and decrease slightly as the water Reynolds number exceeds a value of 25,000. Usually the enthalpy effectiveness shows the performance of the total cooling load removal. The simulation results for the enthalpy effectiveness are higher than the

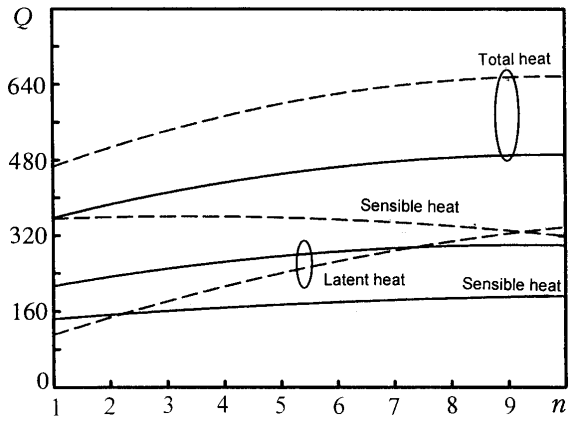

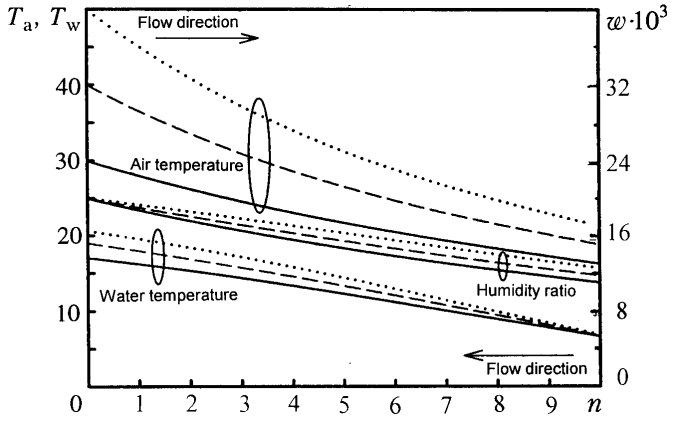

Fig. 6. Variation of heat-transfer rate with number of coil turns at $T_{w,in}$ = 6°C, m_a = 0.25 kg/sec, m_w = 0.1 kg/sec, and w_{in} = 0.02 for different air inlet temperatures: $T_{a,in}$ = 30°C (solid curves) and 50 (dashed curves). Q, W.

Fig. 7. Variation of air temperature, water temperature, and humidity ratio with number of coil turns for different air inlet temperatures: $T_{a,in}$ = 30°C (solid curves), 40 (dashed curves), and 50 (dotted curves). For notation see Fig. 6. T_a, °C; T_w, °C.

experimental data of Ho and Wijeysundera [10], which gives an average error of 1.2%. While the humidity effectiveness shows the latent-load removal performance, these results are higher than those of experimental data, which gives an average error of 4%. It should be noted that the curve characteristics are similar to those of counter and cross flow sensible heat exchangers.

Figure 5a shows the variation of the enthalpy and humidity effectivenesses with the water Reynolds number for different air mass flow rates. It appears that enthalpy and humidity effectivenesses increase with a decrease in the air mass flow rate. This is because the heat capacity of the hot air increases with increasing flow rate. However, because the heat removal capacity of chilled water is kept nearly constant, the outlet air temperature and enthalpy are therefore higher. This results in the decreasing enthalpy and humidity effectivenesses. For the low air-flow-rate region, the humidity effectiveness is higher than the enthalpy effectiveness because the latent heat is more dominant than sensible heat. However, when the air mass flow rate exceeds a value of 0.15 kg/sec, the enthalpy effectiveness is higher than the humidity effectiveness for the low water Reynolds number region.

Figure 5b shows the variation of enthalpy and humidity effectivenesses with the air mass flow rate for different water flow rates. It should be noted that the enthalpy and humidity effectivenesses are inversely proportional to the air mass flow rate. The slope of the graph indicates the decreasing rate of enthalpy and humidity effectivenesses. As the water flow rate increases, enthalpy and humidity effectivenesses also increase. The increase in heat-removal capacity of the water results in a reduction of outlet air humidity ratio and enthalpy.

Figure 6 shows the variation of heat-transfer rate with number of coil turns for different inlet air temperatures. When the coil surface temperature is below the dew-point temperature of the air, heat and mass transfer occur simultaneously. This shows that as the number of coil turns increases, the heat-transfer rate increases to a maximum and then decreases. The total and sensible heat-transfer rates increase with increasing inlet water temperature. The decrease in the temperature gradient between inlet air and water temperatures results in a reduction in heat removal capacity of the water. The latent heat is higher than the sensible heat at an inlet air temperature of 30°C. It is also interesting to note that the sensible heat is higher than the latent heat at an inlet air temperature of 50°C because the sensible heat depends on the temperature gradient between inlet air and tube surface. As the inlet air temperature increases, the sensible heat also increases.

Water and air temperatures as well as humidity ratio increase with increasing inlet air temperature and they are inversely proportional to the number of coil turns, as shown in Fig. 7. The increase in the condensation of water vapor in the moist air, as the inlet air temperature decreases, results in a reduction of the air humidity ratio.

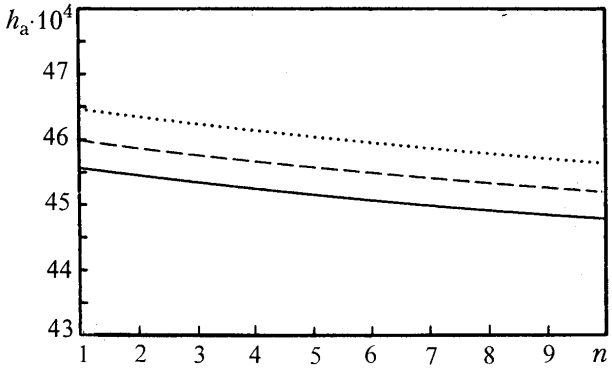

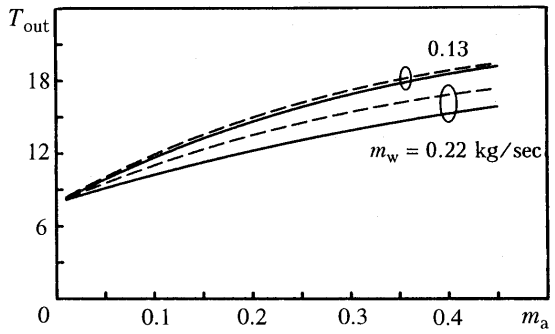

Fig. 8. Variation of air-side heat transfer coefficient with number of coil turns for different air inlet temperatures. For notation see Fig. 7.

Fig. 9. Variation of water (solid curves) and air (dashed curves) outlet temperatures with air flow rate for different water flow rates. For notation see Fig. 5. T_{out}, °C; m_a, kg/sec.

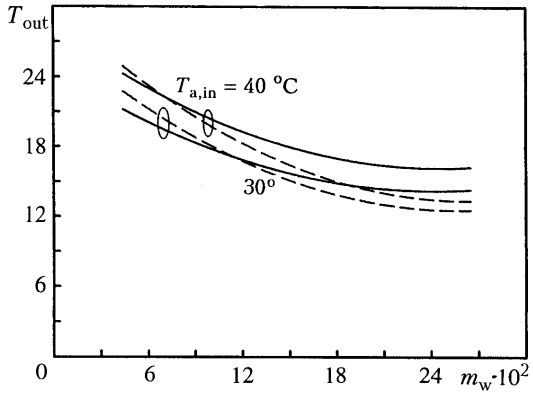

Fig. 10. Variation of water (dashed curves) and air (solid curves) outlet temperatures with water flow rate at $T_{w,in}$ = 8°C, m_a = 0.25 kg/sec, w_{in} = 0.02, and n = 10 for different air inlet temperatures. T_{out}, °C; m_w, kg/sec.

Figure 8 shows the variation of the air-side heat-transfer coefficient with the number of coil turns for different inlet air temperatures. It can be noted that the air-side heat-transfer coefficient decreases with increasing number of coil turns. Generally, the heat-transfer coefficient under wet-surface conditions is higher than that under dry-surface conditions. The decrease in the outlet air temperature of each coil turn results in a reduction of the air-side heat-transfer coefficient. As the inlet air temperature increases, the air-side heat-transfer coefficient increases too. This is due to the fact that the heat-transfer coefficient is directly proportional to the temperature. As the air inlet temperature and water and air flow rates are maintained constant and the inlet water temperature increases, the air-side heat-transfer coefficient increases.

Figure 9 shows the variation of the outlet water and outlet air temperatures with the air mass flow rate. The outlet water and outlet air temperatures increase as the air mass flow rate increases because the heat removal capacity of chilled water is kept nearly constant while the heat capacity of hot air increases. The heat capacity of hot air is also higher than the heat removal capacity of chilled water. Figure 10 shows the variation of outlet water and outlet air temperatures with the water flow rate at different inlet air temperatures. It can be noted that the outlet water and outlet air temperatures decrease rapidly with the water flow rate for low water flow rate region. However, these effects diminish as the water flow rate is further increases. The increase in heat transfer from hot air to chilled water results in a decrease in the outlet air and water temperatures.

Conclusions. The performance and heat-transfer characteristics of spiral-coil finned tube heat exchangers were investigated. It was found that the conditions at the inlet of both working fluids have an effect on the heat and mass transfer and performance of spiral-coil heat exchanger as follows:

– Enthalpy and humidity effectivenesses are inversely proportional to the air mass flow rate.

– Heat-transfer characteristics along the coil turn are functions of inlet properties of both working fluids.

– Latent and sensible heat rates depend on two factors: the tube surface area and the temperature difference between the air and tube surface.

– The effect of inlet water temperature on fin efficiency is very small.

– The air-side heat-transfer coefficient increases with increasing inlet water temperature.

Acknowledgements. The authors would like to express appreciation to the Thailand Research Fund for providing financial support for this study.

NOTATION

A, area, m^2; C_p, specific heat of dry air, kJ/(kg·K); C_{pm}, specific heat of moist air, kJ/(kg·K); C_{pwv}, specific heat of water vapor, kJ/(kg·K); D, diameter of tube, m; D_c, diameter of curvature of coil, m; De, Dean number; E_i, enthalpy effectiveness; E_w, humidity effectiveness; G, mass flux based on minimum free flow area, m_a/A_{min}, kg/(m^2·sec); h_a, air-side heat-transfer coefficient, W/(m^2·K); h_{com}, combined conductance through tube surface and water inside tube, W/(m^2·K); h_i, in-tube heat-transfer coefficient, W/(m^2·K); h_{mass}, mass-transfer coefficient, kg/(m^2·sec); i, enthalpy, kJ/kg; J, Colburn J factor; j, number of segments; k, thermal conductivity, W/(m·K); Le, Lewis number; m, mass flow rate, kg/sec; n, number of turns of coil; Nu, Nusselt number; Pr, Prandtl number; Q, heat-transfer rate, W; r, radius of tube, m; R_f, radius of fins, m; R_{min}, minimum coil radius, m; R_n, average radius of curvature of coil, m; Re, Reynolds number; T, temperature, ^oC; w, humidity ratio, kg_{wv}/kg_a; x, tube thickness, m; y, fin thickness, m; α, rate of change of radius, m/radian; η, fin efficiency; θ, angular position of a point from a fixed line, radians. Subscripts: a, air; ave, average; b, base; c, curvature; con, condensation; cr, critical; f, fin; fs, fin spacing; i, inside; in, inlet; L, latent; m, moist; min, minimum; o, outside; out, outlet; S, sensible; s, surface; sat, saturated; T, total; v, vapor; w, water.

REFERENCES

1. A. M. Jacobi and V. W. Goldschmidt, *Int. J. Heat Mass Transfer*, **33**, 755–765 (1990).
2. Y. Cengiz, B. Yasar, and P. Dursun, *Appl. Energy*, **50**, 85–94 (1995).
3. R. C. Xin, A. Awwad, Z. F. Dong, and M. A. Ebadian, *Int. J. Heat Mass Transfer*, **40**, 482–488 (1997).
4. S. Rahul, S. K. Gupta, and P. M. V. Subbarao, in: *Proc. Third ISHMT–ASME Heat and Mass Transfer Conf. and Fourth National Heat and Mass Transfer Conf.* (1997), pp. 381–385.
5. H. J. Kang, C. X. Lin, and M. A. Ebadian, *Int. J. Heat Mass Transfer*, **43**, 2553–2564 (2000).
6. C. E. Kalb and J. D. Seader, *Int. J. Heat Mass Transfer*, **26**, 23–32 (1983).
7. R. C. Xin and M. A. Ebadian, *J. Heat Transfer*, **119**, 467–473 (1997).
8. J. C. Ho, N. E. Wijeysundera, S. Rajasekar, and T. T. Chandratilleke, *Heat Recovery System & CHP*, **15**, 457–468 (1995).
9. J. C. Ho and N. E. Wijeysundera, *Appl. Therm. Eng.*, **16**, 777–790 (1996).
10. J. C. Ho and N. E. Wijeysundera, *Appl. Therm. Eng.*, **19**, 865–883 (1999).
11. F. C. McQuiston and J. D. Parker, *Heating, Ventilating and Air Conditioning*, John Wiley & Sons, Canada (1994).
12. S. Y. Liang, M. Liu, T. N. Wong, and G. K. Nathan, *Appl. Therm. Eng.*, **19**, 1129–1145 (1999).
13. S. Y. Liang, T. N. Wong, and G. K. Nathan, *Appl. Therm. Eng.*, **20**, 941–962 (2000).